Observation of temperature gradient metamorphism in snow by X-ray computed microtomography: measurement of microstructure parameters and simulation of linear elastic properties

P.K. SRIVASTAVA,[1] P. MAHAJAN,[2] P.K. SATYAWALI,[1] V. KUMAR[1]

[1]*Snow and Avalanche Study Establishment, Him Parisar, Sector 37A, Chandigarh, 160036, India*
E-mail: pks103@rediffmail.com
[2]*Indian Institute of Technology Delhi, Hauz Khas, New Delhi 110016, India*

ABSTRACT. The process of temperature gradient metamorphism in snow strongly affects the microstructure and associated mechanical properties of the snow. The purpose of this study was to: (1) examine the temporal variations in three-dimensional snow microstructure under the influence of a strong temperature gradient for 6 days using X-ray computed microtomography (μCT); and (2) numerically simulate the linear elastic properties of snow from microtomographic data using a voxel-based finite-element technique. The temporal changes in the snow structure were analyzed in terms of density, specific surface area (SSA), thickness distribution of ice matrix and pores, structure model index and mean intercept length (MIL) fabric tensor. The structural indices and orthotropic elastic compliance matrix were computed over several sub-volumes within the reconstructed volume to account for statistical uncertainties. The mean density increased by about 14% on day 1 and no significant trend was observed thereafter. The SSA decreased by 22%, whereas both the ice and pore thickness distributions widened with time. The computed Young's moduli were 1.5–4 times larger than previously published dynamic measurements and found to be significantly correlated with ice volume fraction and MIL fabric measures. The increasing trend in computed moduli during the experiment is consistent with the observed development of thicker vertical ice structures. Multiple linear regression models of elastic compliances using fabric tensor formulation and ice volume fraction could explain 89.9–93.0% of the variance. Our results suggest a strong dependence of elastic properties on both density and microstructural fabric.

INTRODUCTION

Snow is considered as a sintered porous material consisting of an ice matrix and pore space. Temperature gradient (TG) metamorphism, driven by spatial temperature gradients, strongly affects the structural characteristics and produces typical patterns of layering in a natural snow cover (Sturm and others, 1995). The process occurs under conditions of strong vapour transport along a temperature gradient $\sim\geq 10^{\circ}\mathrm{C\,m^{-1}}$ and leads to the development of kinetic growth crystal forms. The kinetic growth crystal forms are classified as 'solid' faceted crystals, which have flat surfaces, or 'skeletal' depth hoar, which has well-developed stepped surfaces and forms vertical chains of hollow cups. Both these depth-hoar forms are generally considered as weak layers as a result of large grain size and reduced degree of intergranular bonding, thereby providing a potential failure plane along lateral horizons for dry-slab avalanche release. Akitaya (1974) observed the formation of a third, very hard, cohesive type of depth hoar, with greater strength characteristics than the solid or skeleton forms, when high-density ($>300\,\mathrm{kg\,m^{-3}}$) snow was exposed to temperature gradients $>39^{\circ}\mathrm{C\,m^{-1}}$. McClung and Schweizer (1999) proposed the stiffness and shear failure toughness of snow to be the important mechanical parameters to consider for the dry-slab release problem. Schweizer and Camponovo (2001) suggested that fracture propagation depends on the difference in stiffness between the weak layer and the slab.

The effective properties of snow, including mechanical properties, depend not only on the density but also on the morphology of ice and pore phase (Schweizer and others, 2003; Kaempfer and others, 2005). Relevant aspects of morphology include density, size measures of ice structures and pores, specific surface area (SSA) and degree of sintering. These features, some of which unfortunately lack precise definition, are used to characterize the snow microstructure. Due to the lack of consistent structural characterization, past attempts were limited to empirical relationships between elastic properties and density. Mellor (1975, 1977) provided the most comprehensive data on elastic properties of snow which include both static and dynamic measurements. However, the data were plotted against snow density since no information on microstructure existed and the values of elastic properties show larger scatter (100–300%). In the recent past, several investigators (Scapozza and Bartelt, 2003; von Moos and others, 2003) have tried to parameterize Young's modulus with density using an exponential relationship, which however is valid only for the investigated fine-grained, well-bonded snow types. These empirical parameterizations provide a convenient way of summarizing the experimental data but lack the rigorous connection with microstructure. Part of the difficulty lies in the fact that two-dimensional (2-D) stereological methods based on planar vertical sections are insufficient to establish reliable correlations between microstructure and mechanical properties (Schneebeli, 2004).

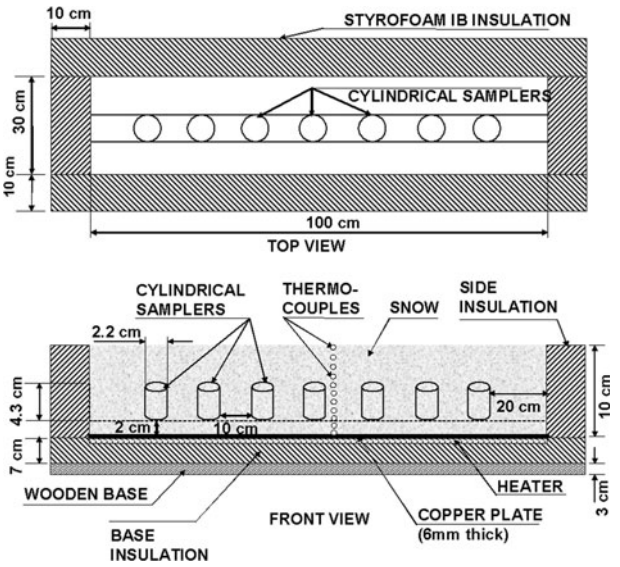

Fig. 1. Schematic of the experimental set-up (top and front views).

An alternative approach is to computationally solve the elasticity equations directly on digital models of microstructure using finite-element (FE) techniques (Garboczi and Day, 1995; Van Rietbergen and others, 1995). Digitized representations of three-dimensional (3-D) microstructure of the material are required as an input to these models. The direct 3-D reconstruction of snow microstructure at resolutions down to a few microns is now possible using technologies such as X-ray computed microtomography (μCT; Coléou and others, 2001; Schneebeli and Sokratov, 2004). Schneebeli (2004) demonstrated the potential of direct FE simulations on 3-D microstructure for the computation of the elastic modulus of TG metamorphosed snow; however, the results were not correlated with the structural changes.

In the present work, TG experiments were conducted in a specially designed apparatus that provided a constant heat flux to the snow sample. Our purpose was to examine the changes in snow microstructure and elastic properties at different stages of metamorphism using μCT imaging. First, we briefly describe the experimental procedure and define the various measures used to characterize the 3-D microstructure. We then describe a voxel-based FE method (Garboczi and Day, 1995) to estimate the linear elastic properties from the tomography data. Finally, we discuss and compare the results of structural and numerical analysis.

EXPERIMENT AND MICROTOMOGRAPHY

Experimental set-up

Snow samples were collected from Patsio research station (32 45′ N; 77 16′ E, 3800 m a.s.l.), Great Himalayan range, India, transported by air to the cold laboratory in insulated boxes and stored at –20°C. This snow was composed of fine grains with an average diameter up to 0.15 mm. A heat-flux apparatus consisting of an insulated box with a copper plate ($1.0 \times 0.30\,m^2$) heated electrically at the base was used for TG experiments. Insulation (100 mm Styrofoam) at the bottom and sides allowed us to maintain a one-dimensional (1-D) heat flow and reduce lateral heat losses. A schematic of the experimental set-up is shown in Figure 1. The detailed design of the apparatus and lateral heat loss analysis is given in Satyawali and others (2008).

The apparatus was initially filled with snow to a height of 2 cm using a 1.0 mm sieve opening. Next, seven thin, cylindrical tubes (diameter ~2.2 cm, height ~4.3 cm, wall thickness ~0.6 mm) were carefully placed vertically on top of the 2-cm snow layer along the length of the heat-flux apparatus. The positions of the cylindrical tubes are shown in Figure 1. The heat-flux apparatus was then again filled with sieved snow very carefully to a total height of 10 cm, such that the cylindrical tubes and the surrounding areas within the apparatus were uniformly packed with snow. Snow temperatures were monitored with type-T thermocouples placed at a regular vertical interval of 1 cm near the centre. The TG experiment was conducted for 6 days in a temperature-controlled cold room maintained at ~–12°C with the snow surface exposed. The temperature at the bottom of the slab was maintained at ~–2°C by the thermostatically controlled copper plate. The average temperature gradient across the snow slab during the experiment was approximately $96^\circ C\,m^{-1}$, with a fluctuation of $\pm 6.2^\circ C\,m^{-1}$ due to fluctuations in cold-room (±0.9°C) and copper-plate (±0.5°C) temperatures. The embedded cylindrical samplers inside the apparatus were carefully extracted on a daily basis to examine the structural changes caused by the applied temperature gradient. The gap created by extraction of the samplers was refilled with similar snow by sieving.

X-ray microtomography imaging

Once sampled, each cylindrical sampler containing snow was weighted to calculate the density (ρ_s) of the snow. After weighing, the sample was imaged with a SKYSCAN 1172 high-resolution X-ray microtomograph. The objective of X-ray absorption tomography is to reconstruct the 3-D internal microstructure from the multiple X-ray shadow projection images recorded at different angular positions of the sample. In this work, 600 projection images covering 180° rotation around the vertical axis were obtained for each sample. The images were acquired with a pixel size of 8.56 μm from the mid-height of the sample. From the projection images, we reconstructed a cubic volume of interest ($900 \times 900 \times 900$ voxels) corresponding to a physical side length of 7.7 mm using modified Feldkamp cone-beam software (NRecon, SKYSCAN).

MICROSTRUCTURE PARAMETERS AND ELASTIC PROPERTIES

Representative elementary volume

The reconstructed 3-D images have an isotropic resolution of 8.56 μm, resulting in $900 \times 900 \times 900$ images, which is a considerable quantity of volumetric data for processing. The resolution of the 3-D images was reduced by a factor of 3 in the three axes ($300 \times 300 \times 300$ voxels) to allow reasonable processing times for the microstructure parameters and the elastic properties computations. Therefore, for all the results presented in this paper, one voxel corresponds to 25.69 μm. The grey-level images were filtered with a 3^3 median filter prior to image reduction. As the grey-level images showed adequate contrast, an automatic threshold using the histogram of the 3-D image dataset was applied to segment the ice and pore phases (Seul and others, 2000).

To limit the computational time, the computational domain for both structural analysis and numerical simulation was chosen based on the following representative elementary

volume (REV) analysis with respect to ice volume fraction (ϕ_i). ϕ_i was calculated using the hexahedral marching cubes volume model (Lorensen and Cline, 1987) of the segmented ice phase. The variation of ϕ_i in cubic sub-volumes of increasing size within the reconstructed volume is shown in Figure 2a. A reasonable estimate for the REV of the investigated snow samples with respect to ϕ_i in this study was 60^3 voxels or $1.54^3\,mm^3$ (Fig. 2a). We selected a computational domain of 100^3 voxels ($\sim 2.57^3\,mm^3$), which is more than four times larger than the minimal REV with respect to ϕ_i, for both the structural analysis and linear elastic properties computations. The structural indices were computed over nine different cubic sub-volumes ($2.57^3\,mm^3$) within each reconstructed volume ($7.7^3\,mm^3$) to account for the statistical uncertainties. The location of sub-volumes within the reconstructed volume is shown in Figure 2b.

Microstructure parameters

The SSA of the ice phase was determined based on the triangulated surface of the marching cubes volume model. The histograms of the local thickness distributions for the ice matrix (with mean structure thickness St_Th) and pores (with mean structure separation St_Sp) were obtained using the distance transform of the ice matrix and pore space, respectively (Hildebrand and Rüegsegger, 1997b; Remy and Thiel, 2002). The structure model index (SMI) was computed based on dilation of the 3-D voxel model (Hildebrand and Rüegsegger, 1997a). The SMI indicates the relative prevalence of rods and plates in the 3-D structure of the ice matrix. The geometrical degree of anisotropy (DA) was determined using the mean intercept length (MIL) method. The MIL is defined as the total length, L, of a line grid divided by the number of intersections between the grid and the ice/pore interface as a function of the grid's orientation (ω): $MIL(\omega) = L/I(\omega)$. The computed mean intercept length values were fitted to an ellipsoid and expressed as the quadratic form of a second-rank tensor **M**, i.e. a fabric tensor (Harrigan and Mann, 1984). The MIL fabric tensor **H** is defined as the inverse square root of **M**. The advantage of using **H** is that larger values of **H** will be associated with larger values of Young's modulus, and that the eigenvalues of **H** are the MIL values in the principal directions (Odgaard and others, 1997). The principal intercept lengths (MIL_1, MIL_2, MIL_3) and the corresponding principal orientations were determined, and ordered such that $MIL_1 > MIL_2 > MIL_3$. The degree of anisotropy is defined as: $DA = MIL_1/MIL_3$.

The effect of resolution (three-fold reduction by resampling) on the evaluation of the structural parameters was tested for the snow samples at day 0 and day 2 (Table 1). Considering the three-fold decrease in resolution, the percentage changes in structural parameters are relatively small. Table 1 also shows the effect of measurement volume on the evaluation of structural parameters at resolution of 25 μm. Considering the 27-fold increase in measurement volume, the changes in structural parameters are relatively very small and our choice of a computational domain of 100^3 voxels seems to fulfil the criterion of REV for the structural parameters considered.

Computation of linear elastic properties

The linear elastic properties of snow were calculated from μCT data using a voxel-based FE programme (Garboczi, 1998). The FE method uses a variational formulation of the linear elastic equations and finds the solution by minimizing the elastic energy using a fast conjugate-gradient technique. To limit uncertainties, FE computations were also carried out over nine different cubic sub-volumes of $2.57^3\,mm^3$ within each reconstructed volume (Fig. 2). The voxels in the μCT datasets were converted directly into trilinear isotropic brick elements. For ice, linear elastic and isotropic properties were specified with a Young's modulus of 9.5 GPa and Poisson's ratio of 0.3 (Sanderson, 1988). Six FE analyses were carried out for each sub-volume considered, with periodic boundary conditions and only one of the six independent strains (ϵ_1, ϵ_2, ϵ_3, ϵ_4, ϵ_5, ϵ_6) non-zero each time. The complete elastic compliance matrix (S_{ijkl}) was then computed from the results of these analyses. Utilizing a numerical optimization procedure, the best orthotropic representation of S_{ijkl} was obtained and Young's moduli (E_1, E_2, E_3) and shear moduli (G_{13}, G_{23}, G_{12}) were calculated (Van Rietbergen and others, 1996).

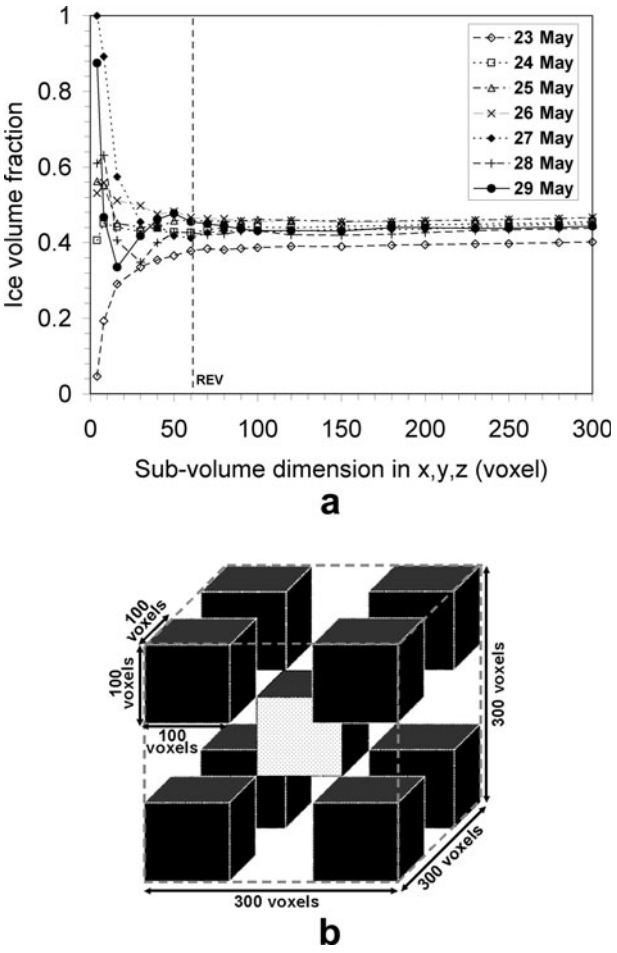

Fig. 2. (a) Variation of ice volume fraction as a function of increasing size of cubic sub-volumes within the reconstructed volume for REV analysis. (b) Locations of nine different sub-volumes ($2.57\,mm^3$) selected within the reconstructed volume ($7.7\,mm^3$) to account for statistical fluctuations.

RESULTS AND DISCUSSION

Microstructural changes under temperature gradient

The 3-D evolution of snow structure under applied temperature gradient is shown in Figure 3. For better visual

Table 1. Effect of the resolution and measurement volume on the evaluation of structural parameters for the day 0 and day 2 snow samples

Structural parameter	Resolution (VOI 300 voxel^3)			Measurement volume (resolution 25.7 μm)		
	8.6 μm	25.7 μm	Change	300^3 voxels	100^3 voxels	Change
ϕ_i, day 0	0.42	0.40	–5%	0.40	0.41 ± 0.01	2.4%
ϕ_i, day 2	0.48	0.47	–2%	0.47	0.47 ± 0.01	<1%
SSA (mm^{-1}), day 0	28.74	28.51	<1%	28.51	29.31 ± 0.56	2.7%
SSA (mm^{-1}), day 2	24.76	24.12	–3%	24.12	25.08 ± 0.64	3.8%
SMI, day 0	1.80	1.73	R–R	1.73	1.86 ± 0.09	R–R
SMI, day 2	0.56	0.52	C–C	0.52	0.87 ± 0.06	C–C
St_Th (mm), day 0	0.143	0.152	7%	0.152	0.151 ± 0.003	<1%
St_Th (mm), day 2	0.142	0.159	12%	0.159	0.158 ± 0.004	<1%
St_Sp (mm), day 0	0.153	0.174	13%	0.174	0.171 ± 0.006	–2.3%
St_Sp (mm), day 2	0.158	0.183	16%	0.183	0.181 ± 0.006	–1.1%
DA, day 0	1.23	1.13	–8%	1.13	1.14 ± 0.02	<1%
DA, day 2	1.54	1.43	–7%	1.43	1.40 ± 0.03	–2.1%

C, coarse; R, round; VOI, volume of interest.

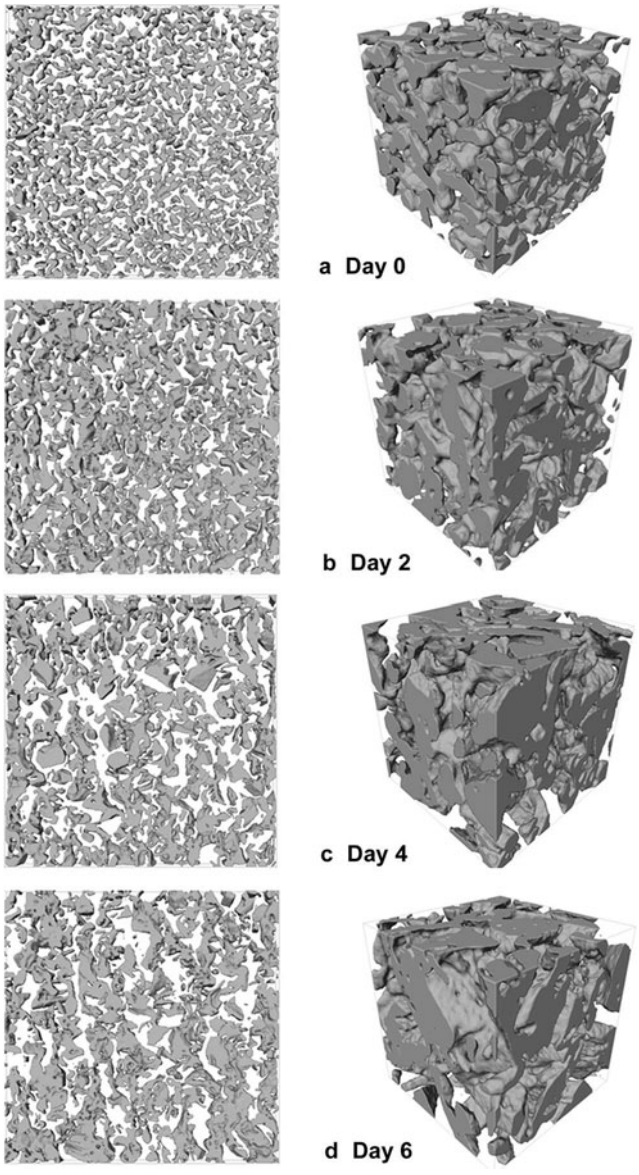

Fig. 3. Temporal changes in 3-D snow structure caused by temperature gradient metamorphism. Vertical slices ($7.7 \times 7.7 \times 0.26$ mm) in the central *y-z* plane along with smaller cubic regions ($\sim 1.71^3$ mm^3), are depicted.

perception, vertical slices ($7.7 \times 7.7 \times 0.26$ mm) in the central *y-z* plane of the complete reconstructed volume along with small sub-volumes (1.74^3 mm^3) are depicted. Visual inspection of the 3-D snow structure indicates a general coarsening along with the development of thicker vertically oriented ice structures, along the direction of the applied temperature gradient.

The temporal variations in mean structural parameters during the experiment are shown in Figure 4. The error bars depicted in Figure 4 reflect ±2 standard error and represent the statistical uncertainties between the analyzed sub-volumes. The statistical fluctuations are less than 2–7% for most of the data points. The density is probably one of the most significant first-order structural parameters of snow and is derived from the ice volume fraction ϕ_i. In this work, we computed ρ_s both by weighting of the cylindrical samplers and from ϕ_i using image analysis of the μCT voxel data. The μCT-based mean density values were higher than those obtained by the weighting method; however, the maximum relative difference was less than 7%. The density of the snow at the start of the experiment was ~ 368 kg m^{-3}. The density varies in a complicated way during the experiment; initially, an increase was observed for the first 2 days and thereafter no significant trend was found (Fig. 4a). A maximum increase of 14% was noted immediately after the application of the temperature gradient on day 1 itself. The variations in structure thickness for ice and pores are depicted in Figure 4b. St_Th increased from an initial value of 0.151 ± 0.003 mm to 0.165 ± 0.004 mm on day 3 and then remained almost constant. St_Sp increased continuously from 0.171 ± 0.006 mm to 0.228 ± 0.008 mm at a much higher rate during the experiment. Figure 4c shows the changes in histograms of the local thickness for the ice matrix and pores. For better clarity, the histograms are shown only for the samples examined at initial day 0 and final day 6. While the pore-space thickness distribution increases and widens continuously, the ice matrix thickness histogram evolves at a much slower rate up to day 3 and hardly changes thereafter.

The changes in principal intercept lengths (MIL_1, MIL_2, MIL_3) of the MIL fabric tensor and the corresponding fabric anisotropy (DA) are shown in Figure 4d and e respectively. The evolution of the principal orientations of the MIL fabric

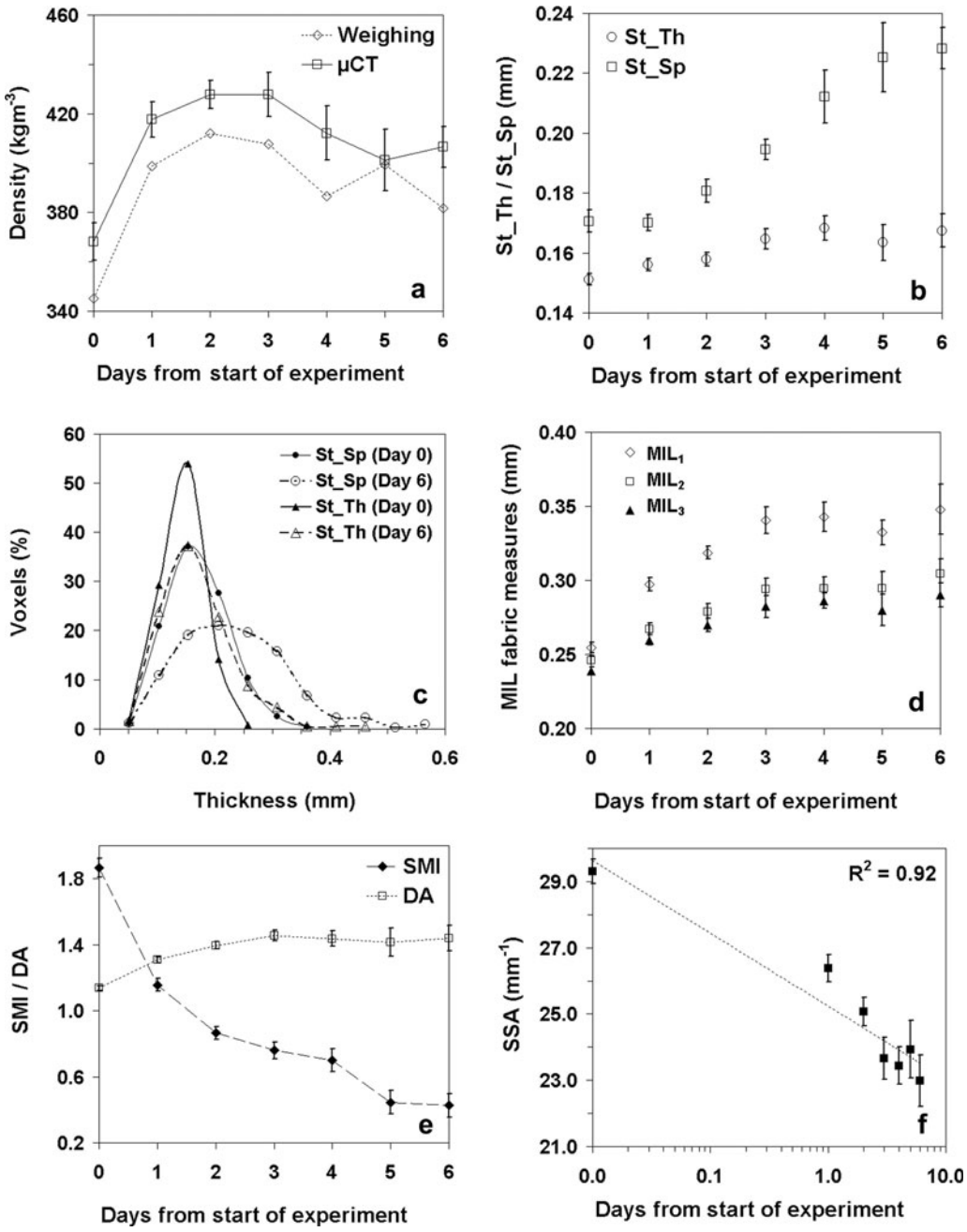

Fig. 4. Changes in the structural parameters during the temperature gradient experiment. (a) Density; (b) mean thickness of ice matrix and pores; (c) histogram of the local thickness for the ice matrix and pores; (d) mean intercept length (MIL) fabric measures; (e) structure model index (SMI) and degree of anisotropy (DA); (f) Specific surface area (SSA).

tensor is given in Table 2. The principal intercept lengths are each an index of the relative length of ice intercepts in each of the three axes described by the orthogonal principal directions. It should be noted that the intercept length may correlate with object thickness in a given orientation but does not measure it directly. The primary direction of MIL fabric tensor (corresponding to MIL_1) aligned itself vertically, i.e. in the direction of the applied temperature gradient within 1 day (Table 2). All three principal intercept lengths increased continuously up to day 3 and reached a plateau, albeit MIL_1 increased at a 1.5- to 2-fold higher rate than MIL_2 and MIL_3. The maximum anisotropy was reached on day 3 and then remained almost constant. The values of MIL fabric tensor measures (Fig. 4d; Table 2) indicate a transversely isotropic fabric ellipsoid with primary orientation along the direction of the applied temperature gradient. It appears that as the structure becomes vertically oriented, the directionally averaged mean structure thickness obtained from the distance transformation method cannot capture the evolution accurately.

The SMI of the ice matrix decreased continuously from 1.86 at the start of the experiment to 0.43 on day 6, which is consistent with the formation of thicker, vertical plate-type ice structures (Fig. 4e). The evolution of SSA during the experiment is presented in Figure 4f. The SSA decreased by ~22% by the end of the experiment, with maximum changes occurring within the first 3 days. Although the experiment was of only 6 days duration, Figure 4e indicates that the decrease in SSA of the ice matrix follows a logarithmic trend quite well.

Table 2. Orthogonal principal orientations (direction cosines) of MIL fabric tensors

Sample	MIL_1 orientation			MIL_2 orientation			MIL_3 orientation		
	i	j	*k*	*i*	*j*	*k*	*i*	*J*	i
Day 0	0.39	0.38	0.84	–0.03	0.92	–0.40	0.92	–0.13	–0.37
Day 1	0.14	–0.06	0.99	–0.13	0.99	0.07	0.98	0.14	–0.13
Day 2	0.09	–0.08	0.99	0.30	0.95	0.05	0.95	–0.29	–0.10
Day 3	0.09	0.01	1.00	0.41	0.91	–0.05	0.91	–0.41	–0.08
Day 4	0.07	0.02	1.00	1.00	–0.03	–0.07	0.03	1.00	–0.02
Day 5	0.10	–0.04	0.99	0.50	0.87	–0.02	0.86	–0.50	–0.11
Day 6	0.25	–0.03	0.97	0.62	0.77	–0.14	0.74	–0.63	–0.21

The observed evolution of various structural parameters during the TG metamorphism in the present work appears to be in line with observations reported by Schneebeli and Sokratov (2004) for the high-density sieved snow, except for the SSA; Schneebeli and Sokratov noted that SSA decreases only for the low-density snow samples, not for the high-density snow samples.

Linear elastic properties

The variations in computed Young's moduli (E_1, E_2, E_3) during the TG experiment are shown in Figure 5a. Like the fabric eigenvalues ($MIL_1 > MIL_2 > MIL_3$), the compliance matrix was sorted such that $E_1 > E_2 > E_3$. Implicitly, it is assumed that the principal mechanical directions are closely aligned with the principal fabric directions. It is interesting to note that the temporal variation pattern of maximum Young's modulus E_1 is closely related with many of the structural indices. The Young's modulus (*E1*), oriented along MIL_1, increases from 459.2 ± 26.2 MPa on day 0 to 1007.0 ± 55.2 MPa on day 3, and thereafter remains more or less constant. The maximum increase in E_1 of more than 100% was observed on day 1 itself. Young's moduli E_2 and E_3 increased by about 40% on day 1 and then slightly decreased to reach a plateau. The similarity in estimated values of E_2 and E_3 indicate a transverse isotropic compliance matrix. The variation in shear moduli (G_{13}, G_{23}, G_{12}) was similar to Young's moduli (Fig. 5b), with maximum changes in shear moduli occurring within 1 day. The error bars depicted in Figure 5 represent the statistical uncertainties between the analyzed sub-volumes.

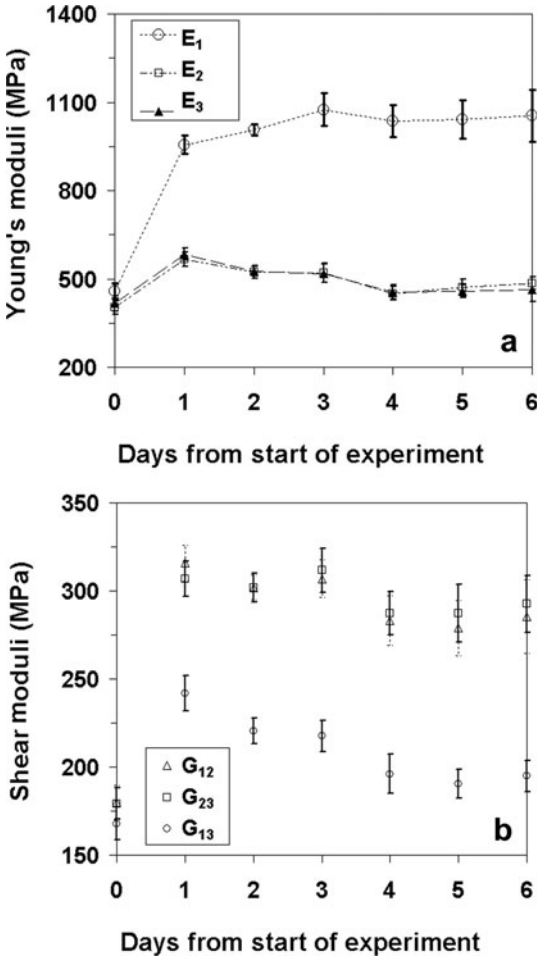

Fig. 5. Variations in computed elastic moduli during the temperature gradient experiment. (a) Young's moduli (E_1, E_2, E_3); (b) Shear moduli (G_1, G_2, G_3).

Schneebeli (2004) computed the evolution of Young's modulus of snow (density –243 kg m^{-3}) in a TG (100°C m^{-1}) experiment using FE analysis of μCT voxel data. He found a substantial decrease (>70%) in axial Young's modulus after 6 days; however, correlations with structural changes were not reported. Although the 3-D structure becomes progressively coarser, the formation of vertical ice structures was not observed (fig. 1 in Schneebeli, 2004). Interestingly, Schneebeli and Sokratov (2004) found that the effective heat conductivity (EHC) of high-density (490–514 kg m^{-3}) sieved snow samples under strong temperature gradients increased immediately; EHC almost doubled from the initial value and reached a plateau at constant density. The increase in EHC was attributed to the formation of thick, vertical ice structures during recrystallization. Akitaya (1974) observed the formation of a very hard, cohesive type of depth hoar when snow ($\rho_s > 300$ kg m^{-3}) was exposed to temperature gradients >39°C m^{-1}. Pfeffer and Mrugala (2002) also demonstrated that hard depth hoar forms from rounded-grain snow ($\rho \geq 400$ kg m^{-3}) following exposure to temperature gradients ≥ 20°C m^{-1}. They characterized hard depth hoar as solid-type depth-hoar grains connected by necks, with vertically preferred directions of grain elongation using horizontal and vertical section planes. The increase in computed elastic moduli during the TG experiment found in the present work is in qualitative agreement with the formation of thicker vertically oriented ice structures (Fig. 3), parallel to the direction of the applied temperature gradient. It appears that both the increase in Young's moduli in the present work and the

Table 3. Non-parametric Spearman's rho correlations (R^2) between mechanical properties and structural parameters

	ϕ_i	SMI	DA	SSA	St_Th	St_Sp	MIL_1	MIL_2	MIL_3
E_1	0.71†	–0.70†	0.76†	–0.64†	0.53†	0.39†	0.70†	0.64†	0.63†
E_2	0.75†	NS	NS	NS	NS	NS	NS	NS	NS
E_3	0.71†	NS	NS	NS	NS	–0.34*	NS	NS	NS
G_{12}	0.87†	–0.39†	0.49†	–0.38†	0.33*	NS	0.42†	0.39†	0.36*
G_{23}	0.82†	–0.46†	0.55†	–0.46†	0.41†	NS	0.50†	0.48†	0.46†
G_{13}	0.80†	NS	NS	NS	NS	NS	NS	NS	NS

*Correlation is significant at the 0.05 level (2-tailed). †Correlation is significant at the 0.01 level (2-tailed).
NS, not significant.

increase in EHC, as reported by Schneebeli and Sokratov (2004), are related to the formation of hard depth-hoar-type structures when high-density sieved snow samples were subjected to high temperature gradients.

Combining entire structural analysis and FE computation datasets, non-parametric Spearman's rho correlation coefficients (R^2) were determined between elastic compliances and 3-D structural indices (Table 3). R^2 gives the proportion of variance explained by the independent variables. Primary Young's modulus (E_1) and shear moduli (G_{12}, G_{23}) were correlated significantly with the structural parameters, unlike E_2, E_3 and G_{13}, which show poor or no significant correlations. In summary, high correlations ($R^2 = 0.71$–0.87) were obtained for the ice volume fraction, and modest to high correlations ($R^2 = 0.3$–0.76) were found for structural parameters. Compared with shear moduli (G_{12}, G_{23}), E_1 was found to be better correlated with MIL fabric measures (MIL_i and DA). Distance transform-based ice and pore-thickness measures, as well as specific surface area, appear to be modestly correlated with elastic moduli. However, it should be noted that the structural parameters considered here are not completely independent and are related to each other.

We have compared our numerical estimates with theoretical Hashin–Shtrikman (HS) bounds (Hashin and Shtrikman, 1963) and previously reported dynamic measurements. The HS bounds are probably the best bounds on the properties of a two-phase composite material without specifying any structural information beyond solid volume fraction or porosity. Figure 6a shows the comparison of the estimated Young's moduli with the upper HS bound and experimental values reported in Maeno and others (1978) from the transversal vibration method. The simulated Young's moduli were 2–8 times less than the theoretical HS bound and 1.5–4 times larger than the dynamic measurements. As such, direct comparison of FE estimates with reported values is difficult because the complete elastic stiffness matrix was not measured for snow and the reported results come mostly from quasi-static compression tests assuming an isotropic material. The error in quasi-static compression tests might obscure the true elastic response and reduce the effective stiffness of the material. Moreover, reported values of effective Young's modulus are strongly dependent on strain rate and our FE analysis does not take into account the strain-rate dependency. Figure 6b shows the comparison of computed shear moduli with the theoretical upper HS bound. The computed G_{ij} values were 3–7 times smaller than the HS bound. The scatter in Figure 6 represents the evolving mechanical anisotropy during the TG experiment.

Developing relationships between material morphology and mechanical properties is of prime importance in many other research areas, such as bone biomechanics. Cowin (1985) developed a polynomial relationship between elastic properties (nine orthotropic elastic constants) and the structure, given by volume fraction and a fabric tensor. Kabel and others (1999) developed constitutive relations of fabric, density and elastic properties in cancellous bone. Based on the elastic-properties–fabric model derived by Cowin, we also attempted to relate the normalized MIL fabric eigenvalues ($\lambda_i = MIL_i/\sum MIL_i$) and ice volume fraction

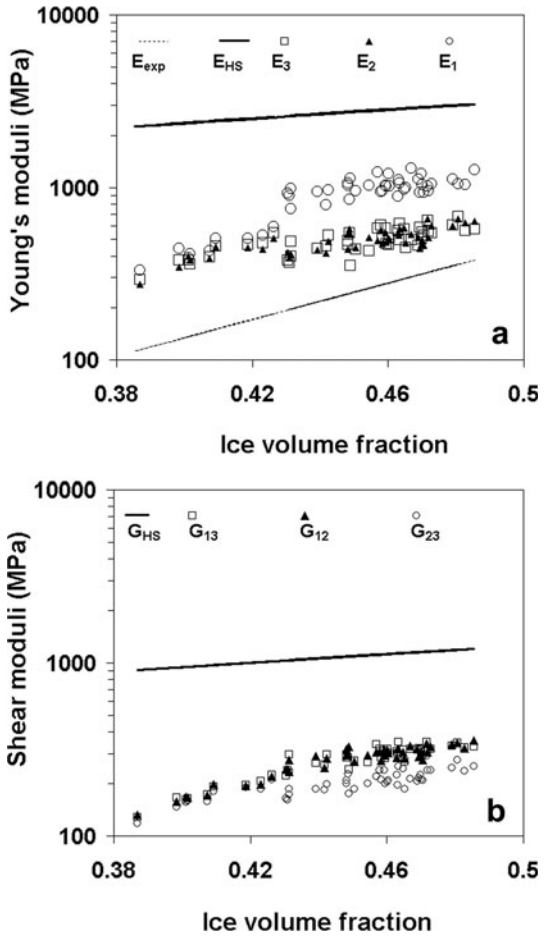

Fig. 6. (a) Comparison of Young's moduli with Hashin–Shtrikman (HS) upper bound (E_{HS}) and dynamic measurements (E_{exp}) of Maeno and others (1978). (b) Comparison of shear moduli with HS upper bound (G_{HS}).

Table 4. Values of constants appearing in regression models (Equation1) obtained from the independent fits

S_{iiii}		S_{iijj}		S_{ijij}	
Parameter	Estimate	Parameter	Estimate	Parameter	Estimate
a_1	455.9	a_2	–45.5	a_3	1261.7
b_1	–69.7	b_2	5.3	b_3	–217.2
c_1	–875.5	c_2	–693.6	c_3	–2834.8
d_1	86.2	d_2	–11.7	d_3	400.3
e_1	–997.6	e_2	825.3	e_3	–980.5
f_1	253.8	f_2	–3.6	f_3	263.9
g_1	1492.4	g_2	–977.3	g_3	1489.2
h_1	–384.4	h_2	39.8	h_3	–405.8
–	–	m_2	–503.2	–	–
–	–	n_2	–71.8	–	–

ϕ_i with the nine orthotropic elastic compliances obtained from the FE analysis. The relationships for the elastic compliances (S_{ijkl}) are:

$$S_{iiii} = \frac{1}{E_i} = \left(a_1 + \frac{b_1}{\phi_i^2}\right) + \left(c_1 + \frac{d_1}{\phi_i^2}\right)\Psi + \left(e_1 + \frac{f_1}{\phi_i^2}\right)\lambda_i + \left(g_1 + \frac{h_1}{\phi_i^2}\right)\lambda_i^2,$$

$$S_{iijj} = \frac{-\nu_{ij}}{E_i} = \left(a_2 + \frac{b_2}{\phi_i^2}\right) + \left(c_2 + \frac{d_2}{\phi_i^2}\right)\Psi + \left(e_2 + \frac{f_2}{\phi_i^2}\right)(\lambda_i + \lambda_j) + \left(g_2 + \frac{h_2}{\phi_i^2}\right)\left(\lambda_i^2 + \lambda_j^2\right) + \left(m_2 + \frac{n_2}{\phi_i^2}\right)\lambda_i\lambda_j,$$

$$S_{ijij} = \frac{1}{G_{ij}} = \left(a_3 + \frac{b_3}{\phi_i^2}\right) + \left(c_3 + \frac{d_3}{\phi_i^2}\right)\Psi + \left(e_3 + \frac{f_3}{\phi_i^2}\right)(\lambda_i + \lambda_j) + \left(g_3 + \frac{h_3}{\phi_i^2}\right)\left(\lambda_i^2 + \lambda_j^2\right), \quad (1)$$

where $i,j = [1, 2, 3]$, $i \neq j$ and $\Psi = \lambda_1\lambda_2 + \lambda_1\lambda_3 + \lambda_2\lambda_3$.

The constants appearing above were calculated by independently fitting each relation using non-linear multiple regression analysis (Table 4). Figure 7 shows the plots between the compliance coefficients obtained from FE analysis and the compliance coefficients predicted by the above relationships. The regression model based on MIL fabric measures and ice volume fraction explained 89.9–93.0% of the variation of the elastic compliances.

Finally, some points regarding three sources of errors, i.e. finite size effects, statistical fluctuations and discretization errors, in the structural and FE analysis should be noted. We have not carried out a detailed error analysis for FE computation due to limitations of computational speed. Structural analysis (Fig. 2a; Table 1) showed that the selected computational volume respects the REV criteria for determination of structural parameters. Correlation analysis (Table 2) suggests that the ice volume fraction is one of the significant parameters controlling the elastic properties. As the computational domain for elastic properties estimation is about four times larger than the minimal REV with respect to ϕ_i, we presume that the finite size errors in FE analysis are also small. Kaempfer and others (2005)

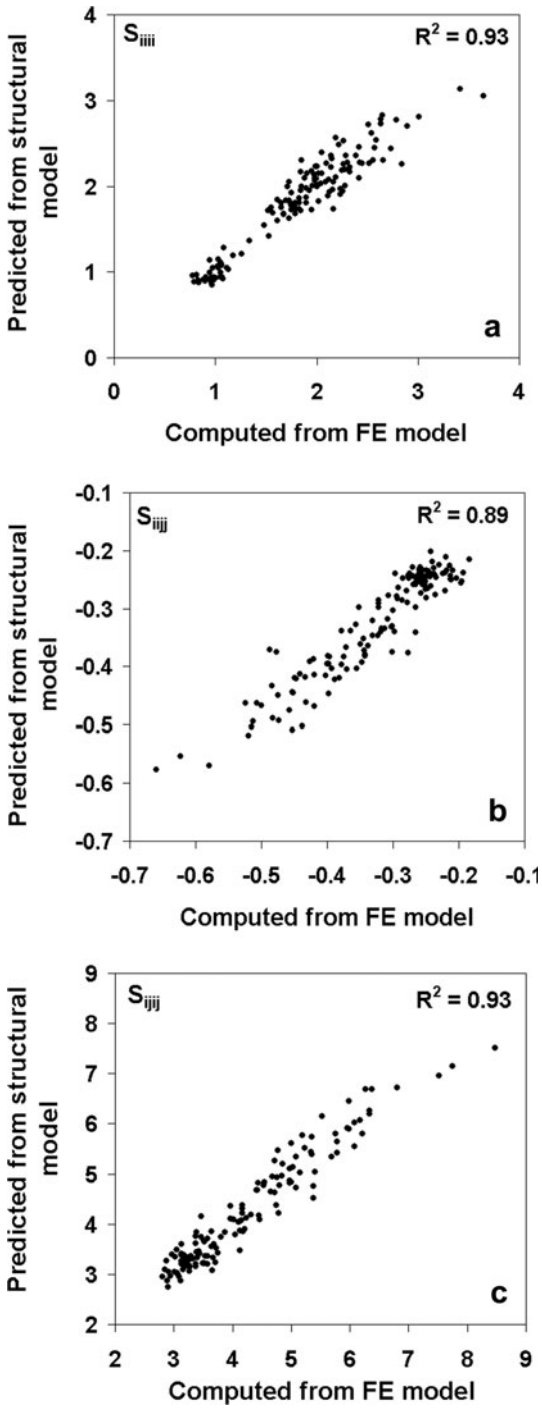

Fig. 7. Correlation between the calculated (from FE technique) and predicted (from regression model) compliance components. (a) S_{iiii}; (b) S_{iijj}; (c) S_{ijij}.

found a REV of 5^3 mm^3 with respect to heat flux in the ice matrix, which is about seven times greater than the computational volume used in this work. Averaging of parameters using nine sub-volumes within the reconstructed volume produces an acceptable level of statistical uncertainties (2–7% for structural parameters and 5–17% for the elastic moduli computation). The discretization error is due to the use of discrete voxels to represent continuum structures. Table 1 shows that the discretization error at a resolution of 25.69 μm is relatively small for the measured structural parameters. Using a periodic open-cell strut model, Roberts and Garboczi (2002) showed that the

discretization errors are <10% if the strut thickness is covered by a minimum of four voxels. In the present work, with the determined minimum mean ice structure thickness of St_Th = 0.151 mm at a resolution of 25.69 μm, we obtained a discretization of a minimum of six voxels per ice structure thickness which meets the criteria established by Roberts and Garboczi (2002).

CONCLUSION

We investigated the temporal variations in 3-D snow structure under the influence of a strong temperature gradient using X-ray μCT imaging. A general coarsening and formation of thicker vertically oriented ice structures along the direction of the applied temperature gradient was observed. The structural analysis suggests that the MIL-based fabric measures are more representative of the evolving anisotropic structure than distance transformation-based thickness measures and indicates a transversely isotropic fabric ellipsoid. The complete orthotropic elastic compliance matrix was computed from the μCT data using a voxel-based FE technique. The elastic properties computed from FE analysis essentially reflect the mechanical properties of snow due to its structure and are not affected by the experimental artifacts. FE analysis thus provided a sound basis for the comparison of elastic properties and the structural variables. The observed increase in computed elastic moduli during the TG experiment is in qualitative agreement with the formation of hard depth-hoar-type vertical ice structures. The computed Young's moduli were found to be 1.5–4 times higher than those reported earlier using dynamic measurements. Other than ice volume fraction (or density), the MIL-based fabric measures appear to be the most significant parameters affecting the elastic properties. Regression models (Equation (1)) of elastic compliances using fabric tensor formulation and ice volume fraction perform exceptionally well and could explain up to 93.0% of the variance in elastic compliances. Although the computational volume with respect to structural analysis and elastic moduli computation was probably too small to reflect the mechanical and structural variability expected in experimental snow samples, they were large enough for the estimation of meaningful relations between snow structure and elastic properties. It is important to note that the FE analysis technique cannot as such replace the traditional mechanical experiments and results should be interpreted only as estimates of elastic properties pertaining to a small snow volume.

ACKNOWLEDGEMENTS

Special thanks to E.J. Garbocji for help with the FE program and Sh A. Ganju for critical comments and discussions. This work was supported by the Defence Research Development Organisation (project No. RDPX-2000/SAS-29).

REFERENCES

Akitaya, E. 1974. Studies on depth hoar. *Contrib. Inst. Low Temp. Sci., Ser. A,* 26.

Coléou, C., B. Lesaffre, J.B. Brzoska, W. Ludwig and E. Boller. 2001. Three-dimensional snow images by X-ray microtomography. *Ann. Glaciol.,* **32**, 75–81.

Cowin, S.C. 1985. The relationship between the elasticity tensor and the fabric tensor. *Mech. Mater.,* **4**(2), 137–147.

Garboczi, E.J. 1998. Finite element and finite difference programs for computing the linear electric and elastic properties of digital images of random materials. Gaithersburgh, MD, National Institute of Standards and Technology NIST Internal Rep 6269.

Garboczi, E.J. and A.R. Day. 1995. An algorithm for computing the effective linear elastic properties of heterogeneous materials: three-dimensional results for composites with equal phase Poisson ratios. *J. Mech. Phys. Solids,* **43**(9), 1349–1362.

Harrigan, T.P. and R.W. Mann. 1984. Characterization of microstructural anisotropy in orthotropic materials using a second rank tensor. *J. Mater. Sci.,* **19**(3), 761–767.

Hashin, Z. and S. Shtrikman. 1963. A variational approach to the theory of the elastic behaviour of multiphase materials. *J. Mech. Phys. Solids,* **11**(2), 127–140.

Hildebrand, T. and P. Rüegsegger. 1997a. A new method for the model-independent assessment of thickness in three-dimensional images. *J. Microsc.,* **185**(1), 67–75.

Hildebrand, T. and P. Rüegsegger. 1997b. Quantification of bone microarchitecture with the structure model index. *Comput. Meth. Biomech. Biomed. Eng.,* **1**(1), 15–23.

Kabel, J., B. van Rietbergen, A. Odgaard and R. Huiskes. 1999. Constitutive relationships of fabric, density, and elastic properties in cancellous bone architecture. *Bone,* **25**(4), 481–486.

Kaempfer, T.U., M. Schneebeli and S.A. Sokratov. 2005. A microstructural approach to model heat transfer in snow. *Geophys. Res. Lett.,* **32**(21), L21503. (10.1029/2005GL023873.)

Lorensen, W.E. and H.E. Cline. 1987. Marching cubes: a high resolution 3-D surface construction algorithm. *Comput. Graph.,* **21**(4), 163–169.

Maeno, N., H. Narita and K. Araoka. 1978. Measurements of air permeability and elastic modulus of snow and firn drilled at Mizuho station, East Antarctica. *Mem. Natl Inst. Polar Res.,* Special Issue 10, 62–76.

McClung, D.M. and J. Schweizer. 1999. Skier triggering, snow temperatures and the stability index for dry-slab avalanche initiation. *J. Glaciol.,* **45**(150), 190–200.

Mellor, M. 1975. A review of basic snow mechanics. *IAHS Publ.* 114 (Symposium at Grindelwald 1974 – *Snow Mechanics*), 251–291.

Mellor, M. 1977. Engineering properties of snow. *J. Glaciol.,* **19**(81), 15–66.

Odgaard, A., J. Kabel, B. van Rietbergen, M. Dalstra and R. Huiskes. 1997. Fabric and elastic principal directions of cancellous bone are closely related. *J. Biomech.,* **30**(5), 487–495.

Pfeffer, W.T. and R. Mrugala. 2002. Temperature gradient and initial snow density as controlling factors in the formation and structure of hard depth hoar. *J. Glaciol.,* **48**(163), 485–494.

Remy, E. and E. Thiel. 2002. Medial axis for chamfer distances: computing look-up tables and neighbourhoods in 2D or 3-D. *Pattern Recog. Lett.,* **223**(6), 649–661.

Roberts, A.P. and E.J. Garboczi. 2002. Elastic properties of model random three-dimensional open-cell solids. *J. Mech. Phys. Solids,* **50**(1), 33–55.

Sanderson, T.J.O. 1988. Mechanical properties of ice: laboratory studies. *In* Sanderson, T.J.O., *ed. Ice mechanics: risks to offshore structures.* London, etc., Graham and Trotman, 70–103.

Satyawali, P.K., A.K. Singh, S.K. Dewali, P. Kumar and V. Kumar. 2008. Time dependence of snow microstructure and associated effective thermal conductivity. *Ann. Glaciol.,* **49**, 43–50.

Scapozza, C. and P. Bartelt. 2003. Triaxial tests on snow at low strain rate. Part II. Constitutive behaviour. *J. Glaciol.,* **49**(164), 91–101.

Schneebeli, M. 2004. Numerical simulation of elastic stress in the microstructure of snow. *Ann. Glaciol.,* **38**, 339–342.

Schneebeli, M. and S.A. Sokratov. 2004. Tomography of temperature gradient metamorphism of snow and associated changes in heat conductivity. *Hydrol. Process.,* **18**(18), 3655–3665.

Schweizer, J. and C. Camponovo. 2001. The skier's zone of influence in triggering slab avalanches. *Ann. Glaciol.,* **32**, 314–320.

Schweizer, J., J.B. Jamieson and M. Schneebeli. 2003. Snow avalanche formation. *Rev. Geophys.,* **41**(4), 1016. (10.1029/2002RG000123.)

Seul, M., L. O'Gorman and M.J. Sammon. 2000. *Practical algorithms for image analysis: descriptions, examples, and code.* Cambridge, etc., Cambridge University Press.

Sturm, M., J. Holmgren and G.E. Liston. 1995. A seasonal snow cover classification scheme for local to global applications. *J. Climate,* **8**(5), 1261–1283.

Van Rietbergen, B., H. Weinans, R. Huiskes and A. Odgaard. 1995. A new method to determine trabecular bone elastic properties and loading using micromechanical finite-element models. *J. Biomech.,* **28**(1), 69–81.

Van Rietbergen, B., A. Odgaard, J. Kabel and R. Huiskes. 1996. Direct mechanics assessment of elastic symmetries and properties of trabecular bone architecture. *J. Biomech.,* **29**(12), 1653–1657.

Von Moos, M., P. Bartelt, A. Zweidler and E. Bleiker. 2003. Triaxial tests on snow at low strain rate. Part I. Experimental device. *J. Glaciol.,* **49**(164), 81–90.